RESEARCH ARTICLE

RSP Science Hub

International Research Journal on Advanced Science Hub
2582-4376
www.rspsciencehub.com
Vol. 07, Issue 12 December

Check for updates

http://dx.doi.org/10.47392/IRJASH.2025.133

Thermal Performance Study of an Electric-Motor Using Innovative Indirect Cooling Methods

Kiran Ragi[1], Dr. V. Sajith[2], Dr. Kumaravel S[3], Basavaraja Meti[4]

[1]PG Scholar - Electrical Engineering, National Institute of Technology, Calicut, Kerala.

[2]Professor, MSED, National Institute of Technology, Calicut, Kerala.

[3]Associate Professor, Department of Electrical Engineering, National Institute of Technology, Calicut, Kerala

[4]Senior Engineer, Bosch Global Software Technologies, Bengaluru, Karnataka.

Email ID: *kiranragi98@gmail.com[1], sajith@nitc.ac.in[2], kumaravel_s@nitc.ac.in[3], Basavaraja.Meti@in.bosch.com[4]*

Article history

Received: 05 October 2025
Accepted: 28 October 2025
Published: 26 December 2025

Keywords:

Meander cooling channel, Helical cooling channel, nanofluids, boron nitride (BN), carbon nanotubes (CNT), thermal performance factor (TPF), indirect liquid cooling, ethylene glycol coolant, pressure drop, saturation point, EV motor cooling enhancement.

Abstract

A 70 kW Permanent Magnet Synchronous Motor (PMSM) is selected for the present thermal management study, where detailed loss calculations including stator iron losses, copper losses, rotor and magnet losses are applied as distributed heat sources in the simulation. A mesh sensitivity analysis is performed, and an optimized mesh configuration with 14 prism layers is adopted to accurately resolve near-wall heat transfer. The numerical model is validated using an energy balance, ensuring the accuracy and reliability of the thermal predictions. Two indirect liquid-cooling strategies helical and meander cooling channels are evaluated using 3D steady state CFD simulations. Although the Helical channel demonstrates approximately 20% higher thermal performance (TPF), the Meander channel is selected for further analysis due to its lower pressure drop, improved flow uniformity, and better suitability for practical motor integration. Thermal enhancement is further explored using BN and CNT nanofluids dispersed in an ethylene-glycol (EG) base fluid. Increasing the BN and CNT nanoparticle concentrations leads to a marked decrease in average temperatures across stator, windings, rotor, and magnets, indicating enhanced heat removal capability. For both nanofluids, the representative maximum reductions achieved are 8.6% at the stator, 7.7% at the slot windings, 7% at the end windings, and approximately 3.2% across the rotor and magnets. An optimal concentration range is observed for both nanofluids. BN shows a clear and substantial improvement up to 6% concentration, beyond which temperature reduction becomes marginal. Similarly, CNT exhibits strong improvement up to 1% concentration, after which further increases result in minimal additional thermal benefit. These results demonstrate that nanofluids significantly enhance PMSM cooling performance, with well-defined saturation limits guiding their effective usage in next-generation EV motor thermal management..

1. Introduction

Electric motors are the core of propulsion in electric vehicles (EVs), where their performance, efficiency, and reliability are directly influenced by how effectively they are thermally managed. During continuous and peak operation, these motors generate considerable heat due to various loss mechanisms such as copper (Joule) losses, iron (core) losses, eddy current losses, and mechanical losses. If not properly dissipated, this heat can lead to excessive temperatures, causing insulation degradation, loss of magnetic properties, reduced efficiency, and ultimately shorter motor lifespan. Conventional cooling approaches such as passive air cooling or surface-mounted liquid jacket often fall short in high power density EV applications. This limitation has led to the development of more advanced cooling strategies, including internal liquid cooling using engineered flow paths such as helical and meander channels. These designs offer enhanced surface area contact and improved flow distribution, enabling more effective heat removal from critical regions like the stator, rotor, and winding zones. The primary goal of motor thermal management is to maintain the motor's temperature within safe operational limits while ensuring compactness, cost-effectiveness, and manufacturability. By optimizing cooling channel geometries and selecting suitable cooling fluid such as water, oil, or nanofluid the thermal performance of EV motors can be significantly improved. This translates into better energy efficiency, higher reliability, and extended motor lifespan. To systematically address these challenges, the project is structured into the following phases: Identification of Heat Losses in EV Motors Quantify and categorize heat losses (copper, iron, eddy current, mechanical) during continuous and peak operation. Cooling Channel Geometry Evaluation Design, simulate, and compare helical and meander cooling channel configurations to assess their thermal performance and effectiveness in extracting heat from motor components.

1.1. Objectives & Scope

The objective of this study is to analyze and improve the thermal performance of a 70 kW PMSM using indirect liquid cooling. Two cooling geometries Helical and Meander channels are first evaluated using ethylene glycol as the base fluid to compare temperature distribution, pressure drop, and overall cooling effectiveness. Based on this comparison, the Meander channel is selected for its lower pressure drop and uniform heat removal. The scope is further extended to investigate coolant enhancement using Boron Nitride (BN) and Carbon Nanotube (CNT) nanofluids at different concentrations. The study examines average and maximum temperatures of stator, slot windings, end windings, rotor, shaft, and magnets, identifies optimal nanoparticle loading, and determines the saturation limits. Pressure drop variations are also quantified to evaluate the trade-off between thermal improvement and hydraulic penalty.

2. Geometry Description

In this study, the thermal behavior of a Permanent Magnet Synchronous Motor (PMSM) is analyzed using a computational model to investigate the motor's cooling efficiency and heat dissipation mechanisms. The motor model includes the rotor, stator, and magnet assembly, all of which are critical components for assessing the motor's thermal performance. For the purpose of this work, a 70kW PMSM motor is used, with a focus on its operating conditions under both normal and extreme load scenarios. The geometry of the motor is constructed in Spaceclaim, with the key components (rotor, stator, housing, and magnet assembly) defined based on standard motor dimensions. The motor consists of the following components:

- Stator: Includes the laminated core, copper windings, and insulation material.
- Rotor: Comprised of the rotor core and permanent magnets.
- End Windings: End windings are modelled as simplified cylindrical volumes to avoid geometric complexity while still capturing the essential thermal behavior.
- Housing: The external casing of the motor, where thermal interfaces to the environment and cooling systems are defined.

The windings are carefully modelled by considering the effective thermal properties derived using a filling factor of 0.7, ensuring that both copper conductors and insulation materials are accurately represented. The Geometry

dimensions are given in the Table1. To enhance thermal performance, two different cooling channel configurations have been selected and evaluated in this study: helical and meander channels. These designs were chosen based on insights from previous research studies and existing motor geometries known for their thermal effectiveness. The selected channels are integrated into the motor housing and analyzed to compare their efficiency in managing heat dissipation and maintaining optimal temperature levels under varying thermal loads.

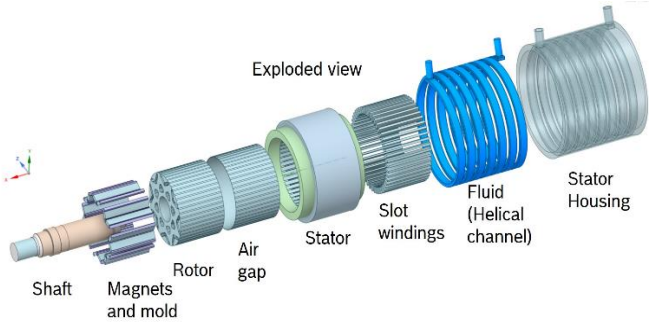

Figure 1 Exploded View Helical Cooling Channel Motor

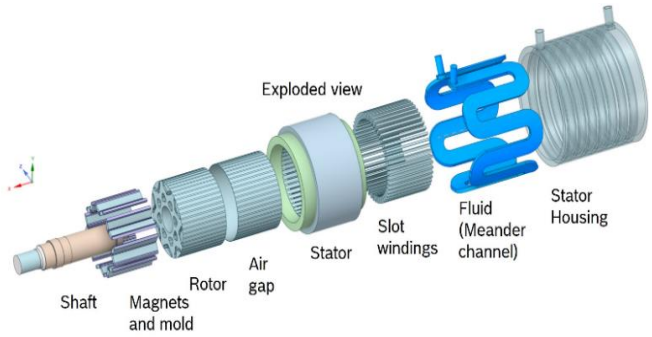

Figure 2 Exploded View Meander Cooling Channel Motor

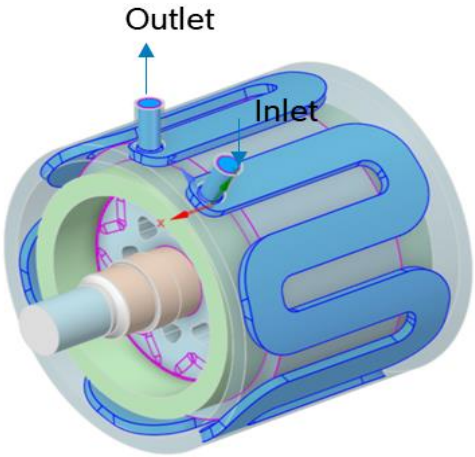

Figure 3 Motor with Meander Cooling Channel

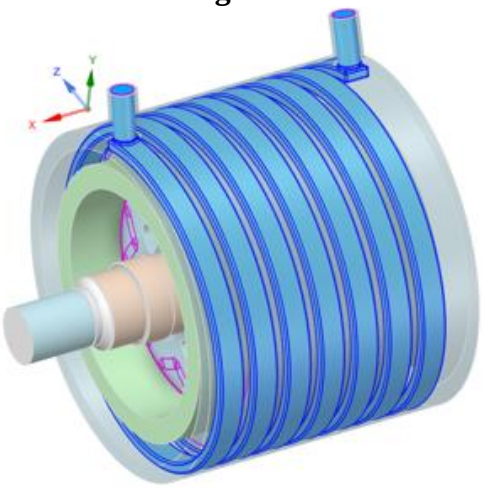

Figure 4 Motor with Helical Cooling Channel

Table 1 Geometrical Dimensions of EV Motor Components

Motor Dimension	Value	Unit
Stator inner diameter	122	mm
Stator outer diameter	170	mm
Slot number	48	-
Axial length of stator	85	mm
Lamination filling factor	0.7	-
Thickness of stator yoke	12	mm
Length of air gap	0.5	mm
Length of magnet	5	mm
Rotor inner diameter	43	mm
Rotor outer diameter	121	mm

3. Heat Loss and Power Dissipation

During the operation of a Permanent Magnet Synchronous Motor (PMSM), various internal components generate heat due to electrical and magnetic losses. Understanding and quantifying these heat sources is essential for accurate thermal modeling and effective cooling system design. The major sources of heat in the motor include: Stator iron loss, which arises due to magnetic hysteresis and eddy currents in the stator core. Copper losses in the slot and end windings, caused by resistive heating (I^2R losses) when current flows through the conductors. Rotor iron loss, which is similar in nature to stator iron loss but occurs in the rotating

part of the motor. Magnet losses, which result from alternating magnetic fields interacting with the permanent magnets The heat loss values for each motor component is shown in Table 2 were obtained from the Tacho simulation tool.

Table 2 Heat Loss Distribution in PMSM Motor

Component	Heat Loss (W)
Stator Iron Loss	1200
Slot Windings Loss	594
End Windings Loss (A side)	241
End Windings Loss (B side)	241
Rotor Iron Loss	75
Magnet Loss	42
Total Heat Loss	2382

Table 4. Properties of Ethylene Glycol

Property	65C	20C
Density [kg/m³]	1048	1074
Specific Heat Cp [J/kg·K]	3454	3201
Thermal Conductivity [W/m·K]	0.406	0.3917
Viscosity [kg/m·s]	0.00129	0.00439

Table 3 Material Properties Used in PMSM Motor Thermal Simulation

Motor Component	Material	Density (kg/m³)	Specific Heat (J/kg.K)	Thermal Conductivity (W/m.K)
Shaft	Steel	7850	490	50
Frame	Aluminum	2650	900	160
Slot windings	Copper (filling factor 0.7)	6230	269.5	273
windings A side	Copper (filling factor 0.5)	4450	192.5	195
windings B side	Copper (filling factor 0.5)	4450	192.5	195
Stator Rotor Lamination	EBG, NO20	7650	490	Radial, tan : 22 Axial : 2.7
Magnet	NdFeB	7550	434	9
Moldmass	Duresco NU 6110 X	2000	1200	0.4
Air gap	Air solid	1.22	900	0.026
Slot Insulation	Mylar Film			0.2

4. Numerical Technique

The PMSM motor's geometric model is created in ANSYS Spaceclaim 2024 R1, and both meshing and simulation are carried out using ANSYS Fluent 2024 R1. ANSYS Fluent's numerical method is based on discretizing the governing equations using the finite volume method, employing a second-order accurate spatial discretization and algebraic multigrid (AMG) techniques to improve convergence. The SIMPLE algorithm is used for pressure–velocity coupling. This method utilizes the relationship between velocity and pressure corrections to obtain the

pressure field and ensure mass conservation throughout the cooling channel domain. The k–ω SST turbulence model is employed, as it provides accurate prediction of both near wall behavior and core flow characteristics in confined cooling passages. For nanofluid modeling, the Mixture Multiphase Model is used, where ethylene glycol is treated as the base fluid and Boron Nitride or Carbon Nanotube nanoparticles are considered as the dispersed secondary phase. This model captures changes in effective density, viscosity, and thermal conductivity due to nanoparticle concentration. A Conjugate Heat Transfer (CHT) approach is adopted to apply the heat losses from stator, windings, rotor, and magnets directly into the solid regions of the motor. The simulation methodology includes a baseline case with pure ethylene glycol, followed by nanofluid cases at different concentrations to evaluate the improvement in thermal performance.

4.1. Governing equations

The numerical model evaluates temperature distribution, heat removal capability, and pressure-drop characteristics for each coolant and geometry, enabling comparison of baseline and nanofluid-enhanced cooling performance. Ethylene glycol–water mixture (EG50/50) is used as the base coolant because of its good thermal stability, high boiling point, wide operating temperature range, and compatibility with aluminum stator housings. To enhance cooling performance, two nanoparticle Boron Nitride (BN) and Carbon Nanotubes (CNT) are evaluated at various concentrations to form nanofluids with improved thermal conductivity. This section discusses the developed simulation model and its boundary conditions.

Fluid Dynamic Model

The simulation model follows the principles of mass, momentum, and energy conservation, which are fundamental to both actual fluid dynamics and CFD numerical simulation.

4.1.1. Conservation of Mass

The law of conservation of mass ensures that the increase in mass of a fluid element per unit time is equal to the net mass flowing into the element per unit time. This is represented by the continuity equation (1), which expresses the mass conservation in fluid flow:

$$\partial\rho/\partial t + \nabla\cdot(\rho\vec{u}) = 0 \qquad (1)$$

Where:

- ρ is the fluid density (kg/m³),
- t is time (s),
- u, v,w are the components of the velocity vector ($\vec{u}$) in the x, y, and z directions (m/s).

4.1.2. Conservation of Momentum

The law of conservation of momentum is derived from Newton's second law, governing the fluid motion. The momentum conservation equation in the x, y, z-directions are expressed as:

$$\partial(\rho u)/\partial t + \nabla\cdot(\rho\vec{u}u) = \nabla\cdot\tau xx + Fx \quad (2)$$

$$\partial(\rho v)/\partial t + \nabla\cdot(\rho\vec{u}v) = \nabla\cdot\tau yy + Fy \quad (3)$$

$$\partial(\rho w)/\partial t + \nabla\cdot(\rho\vec{u}w) = \nabla\cdot\tau zz + Fz \quad (4)$$

Where:

- τxx, τyy, τzz are the components of the viscosity stress tensor (Pa),
- Fx, Fy, Fz are the physical forces on a particle (N).

4.1.3. Conservation of Energy

The conservation of energy, or the first law of thermodynamics for fluid flow, states that the change in internal energy of the flow system is equal to the sum of heat exchange with the surroundings and the work done on the system. The energy equation is expressed as:

$$\partial(\rho uT)/\partial t + \nabla\cdot(\rho uT\vec{u}) = \nabla\cdot(\lambda\nabla T) + S \quad (5)$$

Where:

- cp is the specific heat capacity (J kg−1 K−1),
- T is the temperature (K),

4.2. Mesh Details and Grid Independence Test

A high-quality computational mesh is essential for accurately predicting temperature distribution and coolant flow behavior in the PMSM cooling system. In this study, a polyhedral mesh is used for all simulations due to its superior convergence characteristics and ability to capture complex geometrical features of the motor cooling channels. Separate meshes are generated for the two cooling geometries examined. The total cell count of the mesh is approximately 7 million for the helical channel case and 6 million for the meander channel case These mesh densities provide sufficient resolution to accurately capture fluid flow, thermal gradients, and the detailed coolant pathways within the stator jacket. To resolve near-wall heat transfer accurately, 14 inflation layers with uniform

thickness are applied on all solid–fluid interfaces, including stator housing walls and internal channel surfaces. The selection of 14 layers is based on a mesh sensitivity study, ensuring that results for temperature and pressure drop remain grid independent. A smooth growth rate of 1.2 is maintained to avoid abrupt transitions in element size and to ensure numerical stability. Figure 5 shows Mesh

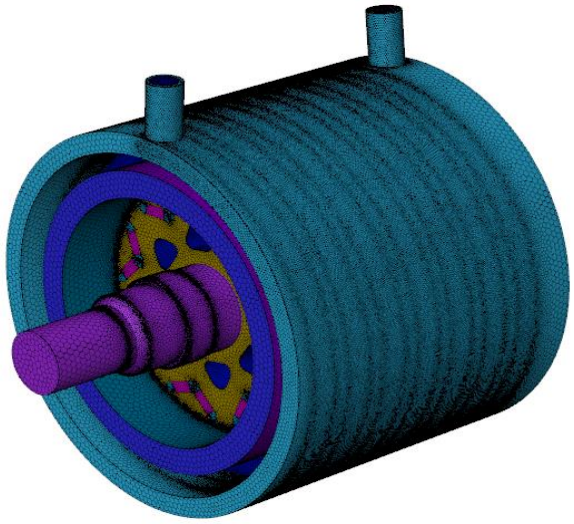

Figure 5 Mesh

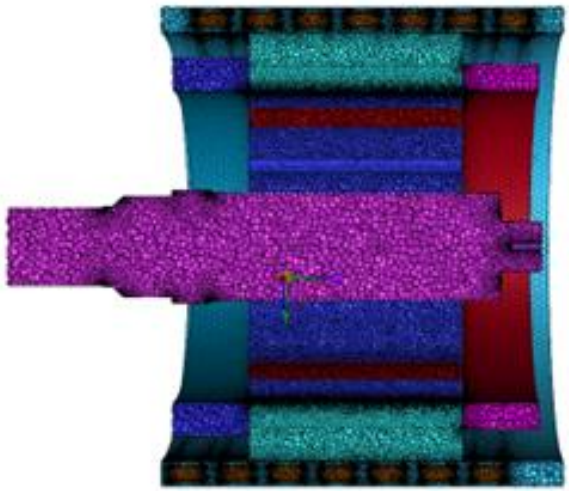

Figure 6 Mesh Section

This meshing strategy combining polyhedral core elements with well-defined inflation layers ensures accurate representation of boundary-layer behavior, improved solution convergence, and reliable prediction of conjugate heat transfer within the PMSM cooling system.

4.3. Boundary Conditions

For the inlet, the coolant is specified with a temperature of 65°C, 20°C and a flow rate of 4, 6, 8, 10 LPM (liters per minute). At the outlet, the conditions are set as a Pressure Outlet with a pressure of 0 Pa, and the backflow temperature is also assumed to be 65°C. These boundary conditions ensure that the coolant flow is properly modeled, allowing the heat transfer process to be accurately simulated within the motor system. Heat Sources and convections are assigned in solids (stator, rotor)

Table 6 Boundary Conditions

Boundary Conditions:	
Inlet	Massflow inlet
Outlet	Pressure outlet - atmospheric pressure
Heat loss @different locations	
Stator Iron loss	1200 [W]
Slot windings	594 [W]
Windings A side	241 [W]
Windings B side	241 [W]
Rotor Iron loss	75 [W]
Magnet loss	42 [W]
Ambient temperature	65 [C]
Natural convection of air	2 [W/m^2K]
Forced convection of air for rotating domains	50 [W/m^2K]

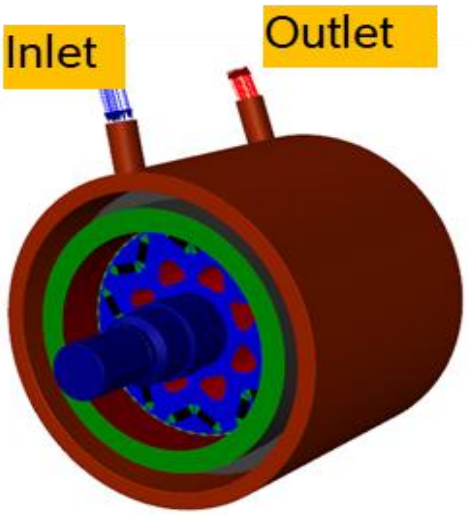

Figure 7 Simulation Model of Helical Channel Motor

Initially, a single-phase steady-state 3D CFD simulation with pure ethylene glycol is carried out to evaluate the baseline cooling channel performance. A steady-state, 3D CFD simulation is performed using the Mixture multiphase model to represent nanofluids, where ethylene glycol acts as the base fluid and BN/CNT serves as the dispersed nanoparticles. The k–ω SST turbulence model is employed to accurately capture near-wall and bulk flow behavior. Further Nanofluids are evaluated with 8lpm 65C standard conditions for different concentrations.

5. Results and Discussion

5.1. Results

The results of the CFD simulations provide valuable insights into the thermal performance of the electric motor under various cooling strategies. For the meander cooling channel configuration, it was observed that the maximum temperature of 164.37°C occurred at the slot windings for a flow rate of 4 liters per minute (LPM) at an inlet temperature of 20°C for the meander channel. Conversely, the minimum temperature of 95.75°C was recorded at the shaft for a higher flow rate of 10 LPM at an inlet temperature of 65°C for the helical channel. These findings underscore the importance of optimizing flow rates to maintain motor temperatures within safe operational limits, particularly noting that the operating

Table 7 Helical and Meander Channel Average Temperature Results

Temperature [C]	Flow rate [LPM]	Cooling channel	Base fluid	Nanoparticle	% Nano particles	Pressure drop [mbar]	Average Temp @ Stator [C]	Average Temp @ Slot Windings	Average Temp @ End windings A	Average Temp @ End windings B	Average Temp @ Rotor	Average Temp @ Magnets	Average Temp @ Shaft	Max Temp @ Slot Windings	Max Temp @ End windings A	Max Temp @ End windings B	Max Temp @ Magnets
65	8	Meander	EG5050	BN	0	102.89	114.13	133.20	139.33	139.38	115.70	123.47	96.61	149.30	148.01	148.01	135.64
65	8	Meander	EG5050	BN	0.5	106.27	107.02	125.85	132.13	132.16	113.06	120.40	95.13	143.02	141.40	141.40	131.98
65	8	Meander	EG5050	BN	1	106.81	106.03	124.83	131.13	131.16	112.70	119.97	94.92	142.16	140.49	140.48	131.48
65	8	Meander	EG5050	BN	2	107.8	105.29	124.06	130.37	130.40	112.42	119.65	94.77	141.51	139.80	139.80	131.09
65	8	Meander	EG5050	BN	3	108.8	104.95	123.71	130.02	130.05	112.30	119.50	94.70	141.22	139.48	139.48	130.92
65	8	Meander	EG5050	BN	6	111.8	104.51	123.25	129.57	129.59	112.14	119.31	94.60	140.84	139.08	139.07	130.69
65	8	Meander	EG5050	BN	10	115.84	104.29	123.02	129.35	129.36	112.05	119.22	94.56	140.65	138.88	138.87	130.58
65	8	Meander	EG5050	CNT	0	102.89	114.13	133.20	139.33	139.38	115.70	123.47	96.61	149.30	148.01	148.01	135.64
65	8	Meander	EG5050	CNT	0.5	106.2	104.91	123.67	129.98	130.01	112.28	119.49	94.69	141.18	139.44	139.44	130.90
65	8	Meander	EG5050	CNT	1	106.77	104.44	123.18	129.51	129.50	112.11	119.29	94.59	140.77	139.01	139.01	130.66
65	8	Meander	EG5050	CNT	2	106.74	104.10	122.83	129.16	129.18	111.99	119.14	94.52	140.48	138.70	138.69	130.48
65	8	Meander	EG5050	CNT	3	108.53	103.96	122.68	129.01	129.03	111.93	119.08	94.49	140.35	138.57	138.56	130.41
65	8	Meander	EG5050	CNT	6	110.99	103.80	122.51	128.85	128.86	111.87	119.01	94.46	140.22	138.42	138.41	130.33
65	8	Meander	EG5051	CNT	10	114.52	103.75	122.46	128.80	128.81	111.86	118.99	94.44	140.19	138.38	138.38	130.30

underscore the importance of optimizing flow rates to maintain motor temperatures within safe operational limits, particularly noting that the operating temperature threshold is 140°C for the insulation copper and 135°C for the magnets. Additionally, the simulations revealed that pressure drop across the cooling channel increases as the flow rates increases and as the temperature increases the pressure drop decreases, indicating a trade-off between enhanced cooling performance and increased pressure requirements. A comparative analysis between Helical and Meander cooling channels was performed at varying coolant temperatures (20°C and 65°C) and flow rates (4LPM to 10LPM). The following observations were made:

Helical Channel demonstrated superior thermal performance:

- Maximum temperature at slot windings reduced from 155.43°C (4 LPM, 20°C) to 143.34 (10 LPM, 65°C).
- Maximum temperature at magnets decreased from 136.88°C to 130.20°C.
- Channel maintained magnet and insulation temperatures below critical thresholds (135°C for magnets, 140°C for windings), especially at higher flow rates.

Meander Channel showed higher peak temperatures, exceeding material limits:

- Slot winding temperature reached a maximum of 164.37°C (4 LPM, 20°C), above Class F (155°C) and Class B (130°C) insulation limits.
- Magnet temperature peaked at 144.06°C, surpassing the 135°C safety threshold for standard NdFeB magnets.
- Increasing flow rate consistently lowered both winding and magnet temperatures in both channels.

Pressure Drop:

- Helical channel exhibited higher pressure

drop (up to 517.14mbar) compared to the Meander channel (194.65mbar at 10 LPM), affecting pump selection and system cost.

To evaluate the relative effectiveness of cooling channels, the Thermal Performance Factor (TPF) is used. It compares the thermal enhancement achieved with increased pumping power (i.e., pressure drop), and is commonly employed in heat exchanger and cooling channel analyses.

Table 8 Average and Maximum Temperature Results of Meander Channel

Temperature [C]	Flow rate [LPM]	Cooling channel	Pressure drop [mbar]	Average Temp @ Stator [C]	Average Temp @ Slot Windings	Average Temp @ End windings A	Average Temp @ End windings B	Average Temp @ Rotor	Average Temp @ Magnets	Average Temp @ Shaft	Max Temp @ Slot Windings	Max Temp @ End windings A	Max Temp @ End windings B	Max Temp @ Magnets
20	4	Helical	129.3	120.38	139.44	144.65	146.43	118.38	124.33	98.50	155.43	153.26	154.62	136.88
20	6	Helical	234.56	116.00	135.03	140.54	141.81	116.78	122.52	97.58	151.19	149.26	150.23	134.61
20	8	Helical	364.09	113.40	132.39	138.07	139.07	115.81	121.42	97.02	148.70	146.88	147.63	133.25
20	10	Helical	517.14	111.60	130.56	136.35	137.18	115.15	120.67	96.64	147.01	145.24	145.86	132.31
65	4	Helical	74.9	114.71	133.66	138.91	140.78	116.27	121.95	97.28	150.21	147.86	149.29	133.94
65	6	Helical	145.43	110.93	129.82	135.40	136.72	114.88	120.37	96.48	146.56	144.46	145.46	131.97
65	8	Helical	236.04	108.86	127.72	133.47	134.50	114.11	119.50	96.03	144.60	142.60	143.38	130.89
65	10	Helical	345.73	107.53	126.36	132.22	133.07	113.62	118.95	95.75	143.34	141.41	142.04	130.20
20	4	Meander	42.38	130.07	149.53	155.37	155.49	121.56	130.30	99.93	164.37	163.52	163.49	144.06
20	6	Meander	82	124.00	143.34	149.26	149.36	119.34	127.71	98.68	158.50	157.52	157.50	140.83
20	8	Meander	121	120.23	139.48	145.46	145.54	117.96	126.10	97.90	154.87	153.80	153.78	138.82
20	10	Meander	194.65	117.69	136.88	142.91	142.98	117.02	125.01	97.37	152.49	151.35	151.33	137.49
65	4	Meander	29.59	121.52	140.76	146.77	146.86	118.41	126.63	98.15	156.37	155.27	155.27	139.56
65	6	Meander	60.95	116.30	135.42	141.51	141.59	116.50	124.40	97.07	151.43	150.19	150.20	136.82
65	8	Meander	102.89	114.13	133.20	139.33	139.38	115.70	123.47	96.61	149.30	148.01	148.01	135.64
65	10	Meander	158.18	111.34	130.34	136.54	136.58	114.67	122.27	96.04	146.77	145.40	145.38	134.21

$$TPF = \frac{\left(\frac{Nu}{Nu_r}\right)}{\left(\frac{\Delta^p}{\Delta p_r}\right)^{\frac{1}{3}}}$$

Nu = Nusselt number (or can be replaced by HTC)
ΔP = Pressure drop
"r" = reference channel (meander)
If we don't have Nu directly, you can estimate it with HTC values, since: $Nu \propto HTC$

The TPF was calculated by using the Meander channel as the reference. The Helical cooling channel exhibited a TPF of approximately 1.2, indicating a 20% improvement in thermal performance per unit pumping power. This suggests that the Helical channel offers improved heat transfer efficiency relative to the associated hydraulic penalty. While the Helical channel demonstrated superior thermal performance (TPF ≈ 1.2), the Meander channel is selected for future studies involving nanofluids and Phase Change Materials (PCMs) due to the following advantages:

- Uniform Heat Distribution: The Meander geometry ensures more uniform cooling, which is critical for evaluating the thermal behavior of advanced materials like nanofluids.
- Lower Pressure Drop: The Meander channel exhibits significantly lower hydraulic resistance, making it more suitable for viscous or multiphase fluids such as nanofluids and PCMs.
- Ease of Fabrication and Integration: Its geometry is simpler to manufacture and integrate, particularly in compact motor housing applications.
- Sensitivity to Enhanced Fluids: Performance gains from nanofluids or PCMs are more clearly observable in geometries with moderate baseline heat transfer,

such as the Meander channel. Therefore, the Meander channel serves as a practical and reliable test platform for evaluating the effectiveness of advanced coolants in electric motor thermal management systems. The subsequent analysis focuses on the thermal performance of BN and CNT nanofluids within the Meander channel configuration. Temperature Distribution The addition of BN nanoparticles to the EG50/50 coolant led to a clear reduction in temperatures across all motor components. At 0% BN, the slot windings exhibited the highest thermal loading with an average temperature of 133.20 °C. As BN concentration increased, a consistent reduction in hotspot temperatures was observed. At 10% BN, the slot winding temperature reduced to 123.02 °C, corresponding to a 10.18 °C drop. Similarly, the end windings showed a significant decline, decreasing from 139.33/139.38 °C at 0% BN to 129.35/129.36 °C at 10% BN. Rotor and magnet temperatures exhibited moderate reductions of approximately 3–

5 °C, while shaft temperatures showed a minor but steady improvement. These results indicate that BN nanofluids enhance both conduction and convection windings. Saturation Behavior of BN Nanofluids: A strong improvement is observed up to 6% BN concentration. Beyond this point, further enhancement becomes marginal, with only 1–2 °C improvement from 6% to 10%. Thus, 6% BN can be identified as the thermally optimal concentration for within the cooling channel, improving the removal of heat from high-loss regions such as slot and end

this geometry and flow condition. Temperature Reduction with CNT Nanofluids: CNT nanofluids showed superior performance compared to BN, delivering lower temperatures in all measured regions

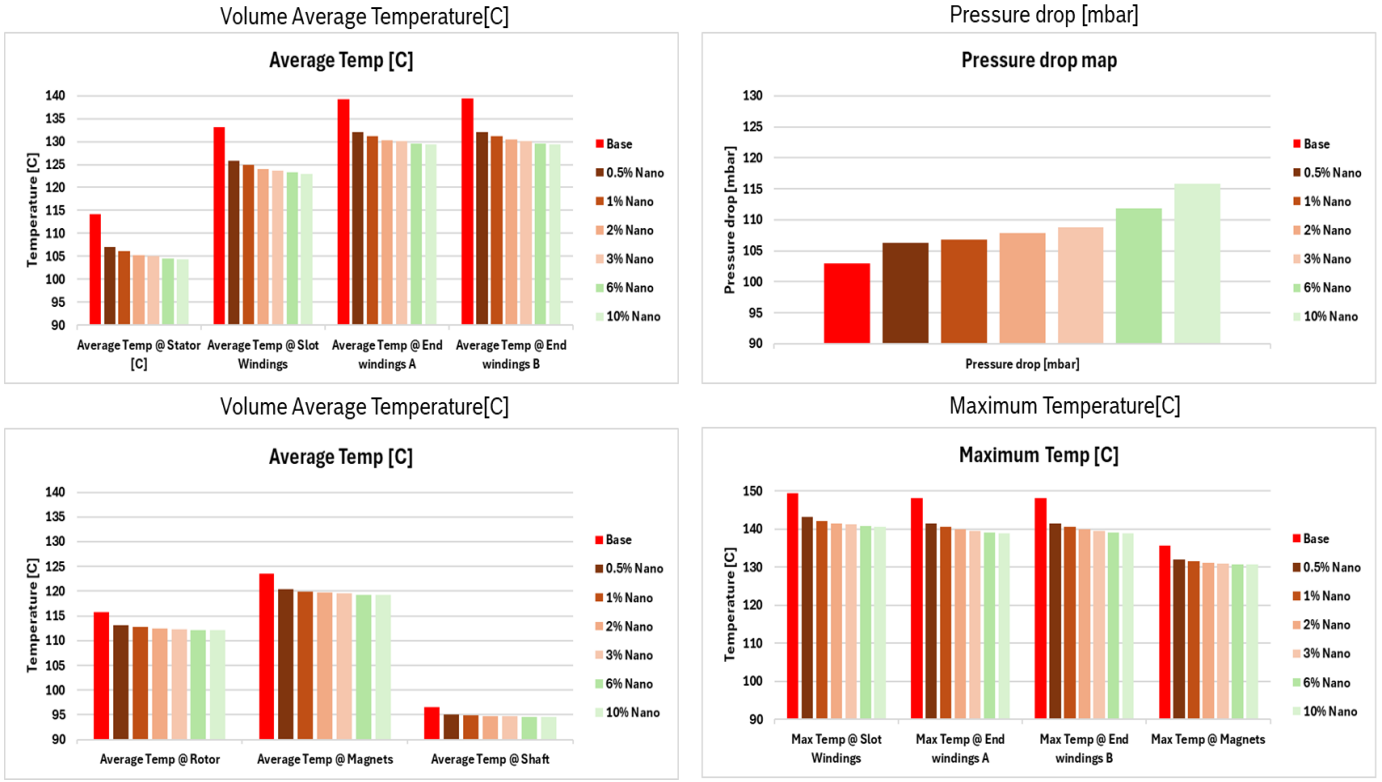

Figure 8 Bar Chart Representing Average Temperature and Pressure Drop for BN Nano fluid

The slot winding temperature reduced from 133.20 °C (0% CNT) to 122.46 °C (10% CNT), giving a 10.74 °C reduction slightly better than BN. End windings, rotor, magnets, and shaft temperatures also followed a continuous downward trend, with 0.3–0.8 °C advantage over BN at similar concentrations. The higher thermal conductivity and aspect ratio of CNTs promote enhanced micro-convection and heat diffusion within the coolant, leading to better thermal performance. Saturation of CNT Nanofluids: Unlike BN, CNT nanofluids showed rapid saturation. A significant portion of the cooling benefit is already achieved at 1% CNT concentration, beyond which the incremental reduction per percentage becomes very small. Although performance improves up to 10%, the gain per concentration beyond 1% CNT is minimal. Thus, CNT exhibits early thermal saturation, while BN shows delayed saturation at 6%.Pressure Drop Analysis Both BN and CNT

addition increased coolant viscosity, causing higher pressure drops. For BN, the pressure drop rose from 102.89 mbar (0%) to 115.84 mbar (10%), while CNT increased to 114.52 mbar (10%). CNT consistently resulted in slightly lower pressure drop at equivalent concentrations, making it more favorable from a hydraulic performance. advanced coolants in electric motor thermal management systems. The subsequent analysis focuses on the thermal performance of BN and CNT nanofluids within the Meander channel configuration. Temperature Distribution The addition of BN nanoparticles to the EG50/50 coolant led to a clear reduction in temperatures

across all motor components. At 0% BN, the slot windings exhibited the highest thermal loading with an average temperature of 133.20 °C. As BN concentration increased, a consistent reduction in hotspot temperatures was observed.

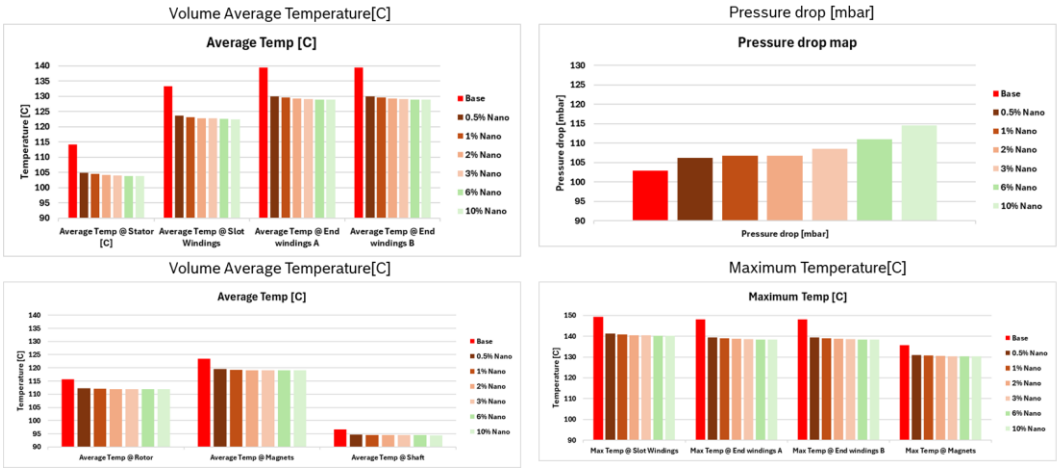

Figure 9 Bar Chart Representing Average Temperature and Pressure Drop for CNT Nanofluid

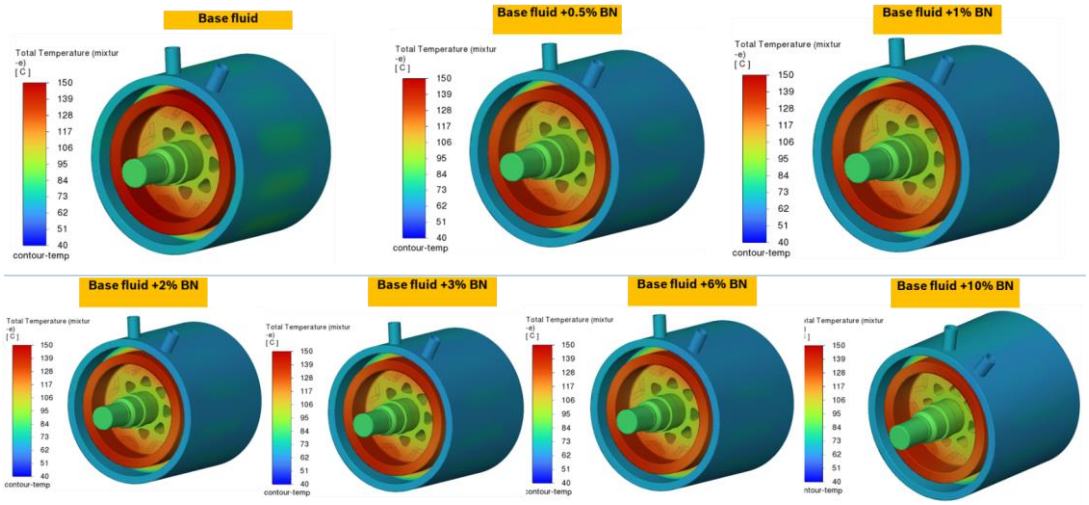

Figure 10 Temperature Contours at Different BN Nano fluid Concentration

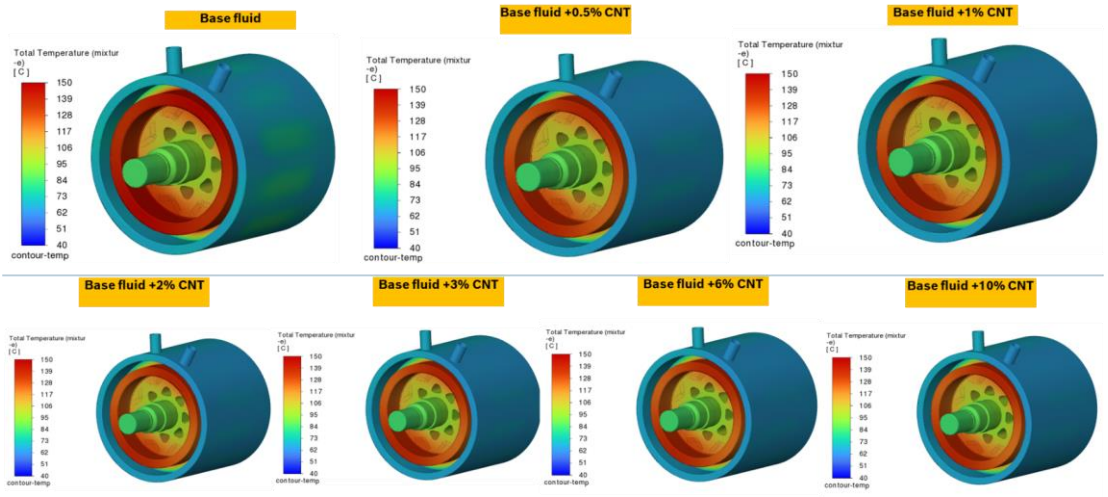

Figure 11 Temperature Contours at Different CNT Nano fluid Concentration

Conclusion

A comparative study of cooling channel configurations was first conducted to identify the most effective geometry for PMSM motor thermal management. Among the assessed designs, the Meander cooling channel demonstrated superior heat removal and more uniform coolant distribution, making it the preferred choice for further investigation. With the channel selection finalized, the focus shifted toward evaluating advanced cooling fluids specifically Boron Nitride (BN) and Carbon Nanotube (CNT) nanofluids to enhance the thermal performance of the EG50/50 coolant. The addition of BN nanoparticles significantly improved heat transfer across all major motor components. Slot winding temperatures reduced from 133.20°C to 123.02°C, and end winding temperatures dropped from 139.33°C/139.38°C to 129.35°C/129.36°C at 10% BN. Rotor and magnet regions showed temperature reductions of 3–5°C, accompanied by a consistent decrease in maximum temperatures, indicating improved thermal dissipation. BN nanofluids showed clear enhancement up to 6% concentration, beyond which thermal gains saturated due to viscosity effects and reduced flow efficiency. Similarly, CNT nanofluids delivered substantial cooling benefits, often outperforming BN. Slot winding temperatures decreased from 133.20°C to 122.46°C, and end winding temperatures reduced to 128.80°C/128.81°C at 10% CNT. Rotor and magnet temperatures also exhibited stronger reductions, typically 4–6°C, with CNT maintaining a slightly lower pressure drop than BN. However, CNT displayed early saturation, with major improvements occurring up to 1% concentration, beyond which further enhancement became marginal. Overall, the combined analysis confirms that while cooling channel geometry establishes the foundation for efficient heat removal, nanofluids substantially elevate thermal performance, with CNT providing the highest temperature reduction and BN offering more stable enhancement over a wider concentration range. These findings demonstrate that nanofluid-enhanced cooling particularly with CNT and BN offers a promising pathway for next-generation electric motor thermal management where improved reliability and thermal efficiency are essential.

Acknowledgements

Place Acknowledgments, including information on the source of any financial support received for the work being published. Place Acknowledgments, including information on the source of any financial support received for the work being published.

References

[1]. Research on Flow and Thermal Coupling Calculation of High-Speed Permanent Magnet Synchronous Motor," 2021 IEEE 12th Energy Conversion Congress & Exposition - Asia (ECCE-Asia), 2021.

[2]. Iron Loss Calculation and Thermal Analysis of High-Speed Permanent Magnet Synchronous Motors Under Various Load Conditions," 2023 26th International Conference on Electrical Machines and Systems (ICEMS), 2023.

[3]. M. Cheng, S. Ding, W. Li, P. Zhang, Q. Wang, and M. Duan, "Cooling System Design and Thermal Analysis of a PMSM for Rail Transit," in Proc. 2020 IEEE 15th Int. Conf. Ind. Electron. Appl. (ICIEA), Kristiansand, Norway, 2020

[4]. P. Lindh, T. Lindh, J. Heikkinen, E. Kurvinen, M. S. De Legarra, and M. Martinez-Iturralde Maiza, "Indirect Water Cooling System Improvements for Vehicle Motor Applications," in Proc. 2015 IEEE 9th Int. Conf. Compat. Power Electron. (CPE), Jun. 2015, doi:10.1109/CPE.2015.7231086

[5]. A. R. Nasr, E. A. Badran, and I. I. Mansy, "Thermal Performance and Sensitivity Analysis of Permanent Magnet Motor: Theoretical Investigation and Optimization," Int. J. Eng. Res. Africa, vol. 72, pp. 13–33, Dec. 2024, doi:10.4028/p-DJ8bke

[6]. Tsibizov, A.; Kovačević-Badstübner, I.; Kakarla, B.; Grossner, U. Accurate Temperature Estimation of SiC Power mosfets Under Extreme Operating Conditions. IEEE Trans. Power Electron. 2020, 35, 1855–1865.

[7]. S. Kharabati and S. Saedodin, “A systematic review of thermal management techniques for electric vehicle batteries,” Journal of Energy Storage, vol. 75. Elsevier Ltd, Jan. 01, 2024. doi: 10.1016/j.est.2023.109586.

[8]. M. M. Hamed, A. El-Tayeb, I. Moukhtar, A. Z. El Dein, and E. H. Abdelhameed, "A review on recent key technologies of lithium-ion battery thermal management: External cooling systems," Results in Engineering, vol. 16. Elsevier B.V., Dec. 01, 2022. doi: 10.1016/j.rineng.2022.1007032

[9]. Thermal Performance of Permanent Magnet Motor: Theoretical Investigation Amany R. Nasr;Ebrahim A. Badran;Ibrahim I. I. Mansy

[10]. M. Cheng, S. Ding, W. Li, P. Zhang, Q. Wang, and M. Duan, "Cooling System Design and Thermal Analysis of a PMSM for Rail Transit," in Proc. IEEE Int. Conf. Industrial Electronics and Applications (ICIEA), 2020.

[11].

[12]. Design and Simulation Analysis of Oil Cooling System for Axial Flux Permanent Magnet Motors Qiping Shen;Li Liu;Hualu Zhu;Tianxiong Zhang;Jianhui Li;Jiaxin Tian

[13]. Quantitative Assessment of Magnet Thickness Impact on PMSM Motor Performance for Evs A Infantraj;G Alfred Jerome;A Andria Morais;R Benita Sharon;R Bennet Vini;V Kirthika

[14]. P. Kim, L. Shi, A. Majumdar, and P. L. McEuen, "Thermal Properties of Carbon Nanotubes and Nanotube-Based Materials," Appl. Phys. A, vol. 74, pp. 113–116, 2002. [Online]. Available: https://link.springer.com/article/10.1007/s003390201277